Journal of Power Sources 256 (2014) 200–205

Contents lists available at ScienceDirect

Journal of Power Sources

journal homepage: www.elsevier.com/locate/jpowsour

Synthesis of porous Co_3O_4 nanoflake array and its temperature behavior as pseudo-capacitor electrode

Y.Q. Zhang, L. Li, S.J. Shi, Q.Q. Xiong, X.Y. Zhao, X.L. Wang, C.D. Gu, J.P. Tu*

State Key Laboratory of Silicon Materials, Key Laboratory of Advanced Materials and Applications for Batteries of Zhejiang Province, and Department of Materials Science and Engineering, Zhejiang University, Zheda Road, No.38, Hangzhou 310027, China

HIGHLIGHTS

- Porous Co_3O_4 nanoflake arrays film is studied as cathode for capacitor in 2 M KOH.
- The porous Co_3O_4 nanoflake arrays film possesses large surface area (105 $m^2\ g^{-1}$).
- Temperature has a pronounced influence for the electrochemical performance.
- Proposed the degradation mechanism of the Co_3O_4 nanoflake arrays film.

ARTICLE INFO

Article history:
Received 25 November 2013
Received in revised form
25 December 2013
Accepted 14 January 2014
Available online 24 January 2014

Keywords:
Tricobalt tetraoxide
Pseudo-capacitor
Aqueous electrolyte
Temperature behavior

ABSTRACT

A porous Co_3O_4 nanoflake array film grown on nickel foam is prepared by a hydrothermal synthesis for pseudo-capacitor application. The pseudocapacitive behavior of the Co_3O_4 nanoflake array is investigated by cyclic voltammograms (CV), galvanostatic charge–discharge tests and electrochemical impedance spectroscopy (EIS) in 2 M KOH at different temperatures. The specific capacity is 210, 289 and 351 F g^{-1} at 2 A g^{-1} tested at −5 °C, 25 °C and 60 °C, respectively, corresponding to that of 184, 243 and 242 F g^{-1} at 20 A g^{-1}. After 4000 cycles at 2 A g^{-1}, the remaining specific capacity is 187, 342 and 124 F g^{-1} tested at −5 °C, 25 °C and 60 °C. It shows that with increasing the temperature from −5 °C to 60 °C, the specific capacity increases, while the cycling stability becomes worse. The operation temperature has a pronounced influence on the pseudocapacitive performance of Co_3O_4 nanoflake array.

1. Introduction

Electrochemical capacitors (ECs), also known as supercapacitors, have attracted increased interest due to their high power density, long cycle life and high density. As one of emerging energy storage devices, ECs have shown the potential to combine the high energy density of batteries and the power density of conventional capacitors. With respect to the charge-storage mechanism, supercapacitors are divided into two kinds: electric double layer capacitor (EDLC) and pseudo-capacitor [1–5]. The EDLC stores energy by rapid adsorption/desorption of electrolyte ions on high specific surface area electrode, which commonly is carbon materials. While in the pseudo-capacitor, charge is stored and released in a Faradic electron-transfer process of metal oxides/hydroxides, conducting polymer or their composites [6,7].

In order to improve the specific capacitance of pseudo-capacitor, metal oxides, such as RuO_2 [8–11], MnO_2 [4,12–18], Co_3O_4 [19–26] and NiO [26–31], have been attracted extensively study due to their high capacitances which are several times larger than carbonaceous materials. Synthesizing high specific surface area materials with different nanostructure to improve the specific capacitance is one of the most important and useful method. For example, nanowires [32–35], nanoflakes [36–40], and core/shell structure metal oxides/hydroxides [4,21,41–43] have been reported. Among the explored active materials of ECs, Co_3O_4 is one of particular interest owing to its easy availability, cost effectiveness, and good pseudo-capacitive behavior. Until now, there has been a variety of reports about the synthesis of different Co_3O_4 nanostructures and their application in pseudo-capacitors [21,22,44,45]. Xia et al. [21] reported a facile hydrothermal synthesis for the large-area growth of self-supported Co_3O_4 nanowire array. The hollow Co_3O_4 nanowire array exhibits superior electrochemical performance with high specific capacitances (599 F g^{-1} at 2 A g^{-1} and 439 F g^{-1} at 40 A g^{-1}) and excellent cycle life. Rao' group [45]

* Corresponding author. Tel.: +86 571 87952573; fax: +86 571 87952856.
E-mail addresses: tujp@zju.edu.cn, tujplab@zju.edu.cn (J.P. Tu).

0378-7753/$ – see front matter © 2014 Elsevier B.V. All rights reserved.
http://dx.doi.org/10.1016/j.jpowsour.2014.01.073

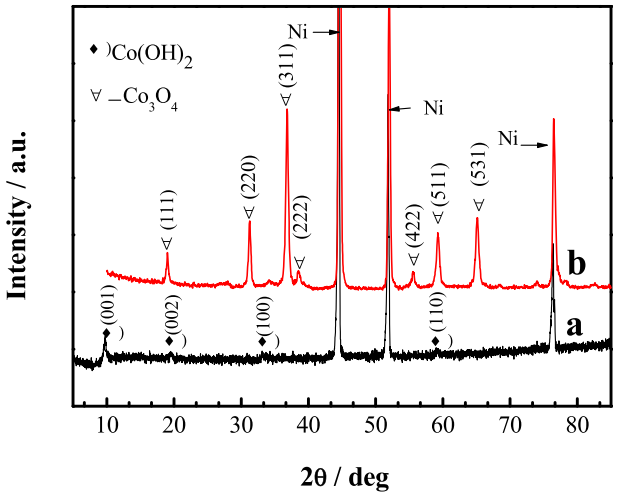

Fig. 1. XRD patterns of films: (a) before and (b) after heat treatment.

synthesized ultralayered Co_3O_4 structures with high porosity by a facile homogeneous precipitation process under hydrothermal conditions. The as-prepared material is capable of delivering very high specific capacitance of 548 F g^{-1} at 8 A g^{-1} and retains 66% of capacitance at 32 A g^{-1}.

Apart from the electrode materials, electrolyte is also one of the key components to influence the electrochemical performance of pseudo-capacitors [46,47]. The attainable cell voltage of a pseudo-capacitor depends upon the breakdown voltage of the electrolyte, and hence the possible energy density (which is dependent on voltage) is limited by the electrolyte. Power density depends upon the equivalent series resistance (ESR) of cell that is strongly dependent on electrolyte conductivity. Aqueous electrolyte is extensively used because of its low cost and high conductivity; especially it does not need operation in dry environment. However, in consideration of the freezing and boiling point of water, operation temperature has an immediately relevance to the electrochemical performance [6,48]. Up to now, there is little literature on the pseudocapacitive performance of the metal oxides employed at different temperatures with aqueous electrolyte. Besides, our group has studied the pseudocapacitive properties of porous $Co(OH)_2$ nanoflake array [49] and the lithium storage performances of Co_3O_4 nanoflake array [50]. Herein, the pseudo-capacitive behaviors of porous Co_3O_4 nanoflake array as a pseudo-capacitor cathode are investigated at different temperatures. These results indicate that the operation temperature has a pronounced influence on its electrochemical performance.

2. Experimental

Cobalt nitrate [$Co(NO_3)_2{\cdot}6(H_2O)$], hexamethylenetetramine ($C_6H_{12}N_4$) and potassium hydroxide were of analytical grade and used without further purification. All aqueous solutions were freshly prepared with deionized water. The nickel foam substrate with a size of 2 cm × 3 cm was cleaned ultrasonically in ethanol for 10 min. Its top side was protected from solution contamination by uniformly coating with a polytetrafluoroethylene tape. The reaction bath for the deposition of $Co(OH)_2$ precursor contained 0.2 M $Co(NO_3)_2{\cdot}6(H_2O)$, and 0.1 M $C_6H_{12}N_4$. The cleaned nickel foam substrates were immersed vertically in the deposition bath. Deposition was carried out at 100 °C for 5 h. After the deposition, the precursor films were washed by deionized water and alcohol, dried in oven at 60 °C, and then heated in a tube furnace at 250 °C for 2 h in flowing argon to obtain final product Co_3O_4. The average loading of Co_3O_4 is determined to be 3.4 mg cm^{-2}, which is calculated by measuring the nickel foam substrate before and after the deposition via a DENVER TB-25 analytical balance.

The structure and morphology of the films were characterized by X-ray diffraction (XRD, PANalytical/X'Pert PRO), scanning electron microscopy (SEM, Philips-FEI/SIRION-100), X-ray photoelectron spectroscopy (XPS, PHI 5700) and transmission electron microscopy (TEM, FEI tecnai G2 F20). The ionic conductivity of 2 M KOH at different temperature was tested by Rex portable conductivity meter (INESA INSTRUMENT). Electrochemical measurements were performed on a CHI660e electrochemical workstation (Chenhua, Shanghai) in a three-electrode electrochemical cell containing 2 M KOH aqueous electrolyte at different temperatures, with the porous Co_3O_4 nanoflake array film as the working electrode, Hg/HgO as the reference electrode and a Pt foil as the counter electrode.

3. Results and discussion

Fig. 1 shows the XRD patterns of the as-prepared nickel foam supporting films before and after heat treatment. Besides the three strong peaks from the Ni foam substrate, all the diffraction peaks in pattern (a) correspond to well-crystallized α-$Co(OH)_2$ phase (JCPDS 74-1057). In pattern (b), the diffraction peaks of the film after heat treatment at 250 °C can be well indexed to a pure cubic phase of Co_3O_4 with Fd3m space group (JCPDS card No. 43-1003).

The morphologies of Co_3O_4 film grown on Ni foam substrate are shown in Fig. 2. Notice that the Ni foam substrate is uniformly covered by interconnected Co_3O_4 nanoflakes (Fig. 2a). These nanoflakes, which are approximately 10 nm in thickness, are generally perpendicular to the substrate and interconnected with each other, forming a highly open net-structure (Fig. 2b). To further characterize the Co_3O_4 nanoflake, the sample is evaluated by TEM

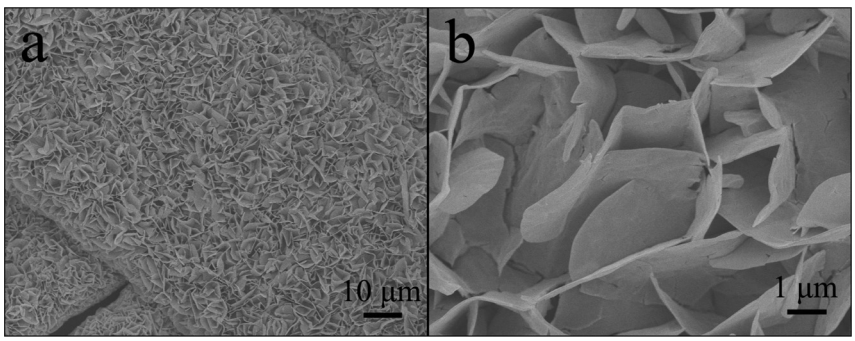

Fig. 2. SEM images of porous Co_3O_4 nanoflake array.

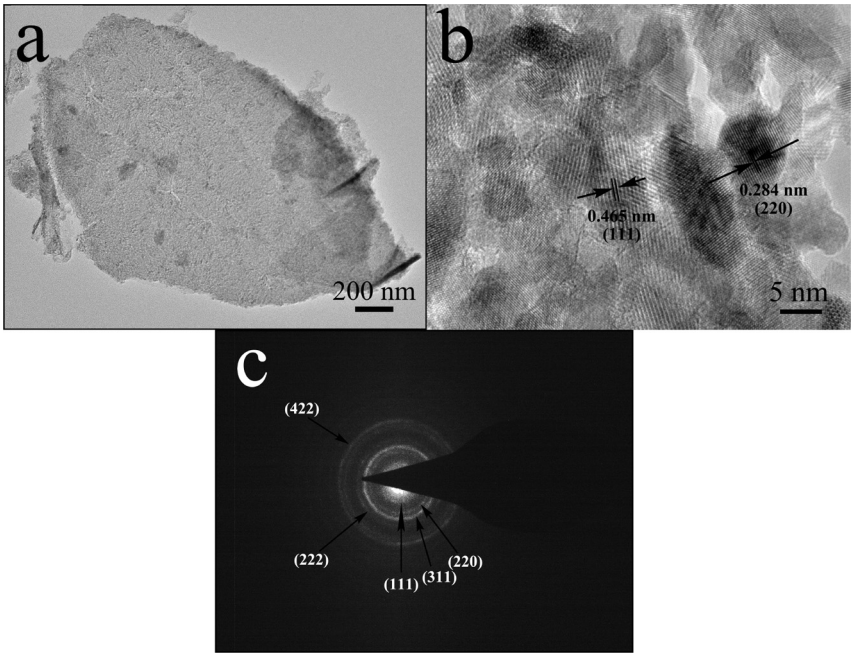

Fig. 3. (a) TEM image, (b) HRTEM and (c) SAED pattern of porous Co_3O_4 nanoflake.

(Fig. 3). As shown in Fig. 3a, the surface of the Co_3O_4 nanoflake is basically smooth. The Co_3O_4 nanoflake is composed by numerous interconnect nanoparticles with a diameter of around 5 nm, which is confirmed by the magnification image (Fig. 3b). The measured lattice spacings of 0.284 and 0.465 nm are in good agreement with the (220) and (111) interplanar distances of cubic phase of Co_3O_4, which coincides with the result of XRD. Similar result is obtained from the SAED pattern in Fig. 3c. The HRTEM and the diffraction rings in the SAED pattern indicate that the Co_3O_4 nanoflake is polycrystalline in nature.

The chemical composition of the film can be further analyzed by XPS. Fig. 4a shows the deconvoluted Co 2p spectrum. Two strong peaks at 794.5 eV for Co $2p_{1/2}$ and 779.8 eV for Co $2p_{3/2}$ are observed. The XPS spectrum of the Co 2p confirms that cobalt exists in the form of Co_3O_4. The O 1s peaks at 529.5 and 531.3 eV correspond to the oxygen species in Co_3O_4 (Fig. 4b). According to the BET analysis, the specific area of the porous nanoflake array is 105 $m^2\ g^{-1}$ (Fig. 5). It has been widely confirmed that this kind of array structure can absorb and strongly retain electrolyte ions, ensuring sufficient Faradic reactions, especially at high current densities.

The electrochemical performances of the Co_3O_4 array film as a pseudo-capacitor electrode are investigated by CV, EIS and galvanostatic charge/discharge tests. The capacitance characteristic of the Co_3O_4 array is that of typical pseudo-capacitance arising from reversible surface or near-surface Faradic reactions for charge

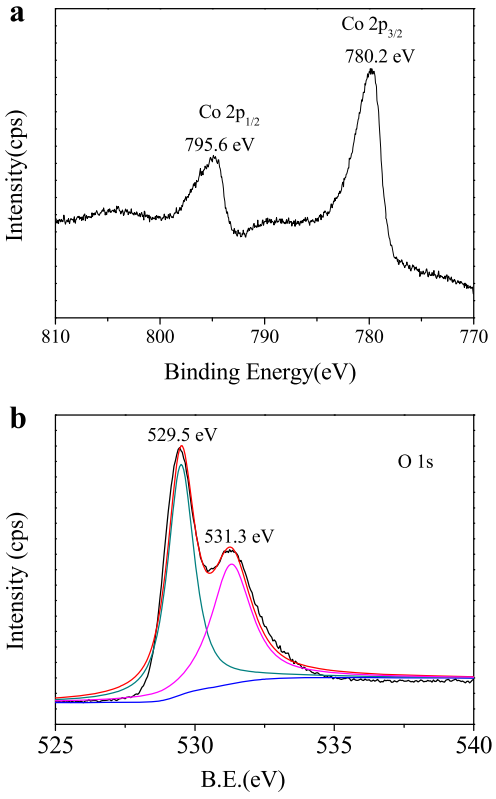

Fig. 4. XPS spectra for Co 2p (a) and O 1s (b) of porous Co_3O_4 nanoflake array.

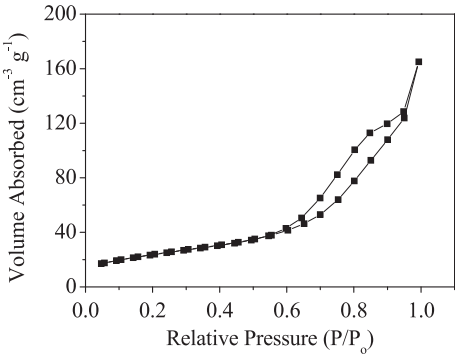

Fig. 5. BET measurements of porous Co_3O_4 nanoflake array.

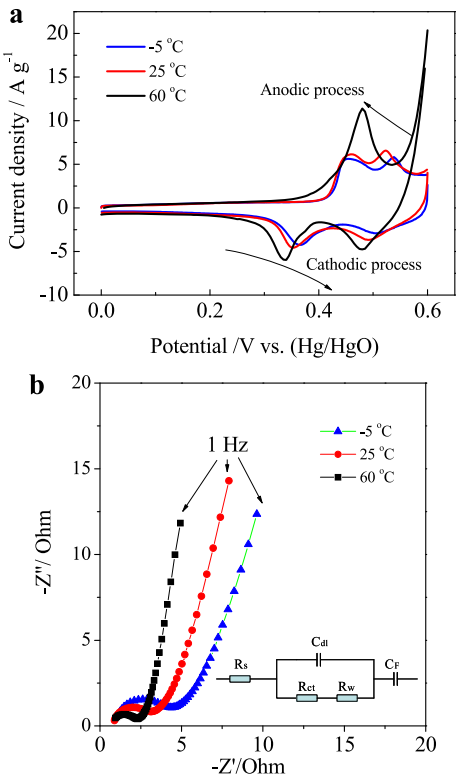

Fig. 6. (a) CV and (b) EIS curves of porous Co_3O_4 nanoflake array electrode at different temperatures (equivalent circuit in inset).

storage. Fig. 6a shows the CV curves of the Co_3O_4 array at a scan rate of 20 mV s^{-1} at different temperatures. When tested at −5 °C and 25 °C, two typical redox couples are noticed in the CV curves. The first redox couple A_1/C_1 is attributed to the conversion between Co_3O_4 and CoOOH, expressed as follows:

$$Co_3O_4 + OH^- + H_2O \leftrightarrow CoOOH + e^- \quad (1)$$

The second redox couple A_2/C_2 corresponds to the reversible reaction between CoOOH and CoO_2, represented by the following reaction:

$$CoOOH + OH^- \leftrightarrow CoO_2 + H_2O + e^- \quad (2)$$

With increasing the operation temperature, A_1 and A_2 move towards each other. As the temperature increases to 60 °C, they combine into one peak. This phenomenon is probably mainly due to the more electrode materials taking part in reaction with the increase of the operating temperature. When A_2 process starts, A_1 hasn't finished yet. So they combine into one peak. The curve at 25 °C also shows that the two peaks are closer with each other compared with that at −5 °C. And both the oxidation peaks move to low potential when the operation temperature increases. As shown in the CV curves, the reaction range at 60 °C is 0–0.5 V rather than 0–0.55 V which is the reaction range at −5 °C and 25 °C. In addition, the higher the temperature is, the higher the peak current density is, indicating higher electrochemical activity and more active materials participating in the redox reaction. It is suggested that the operation temperature has an obvious influence on the electrochemical reaction.

Table 1
EIS parameters of Co_3O_4 array electrode at different temperatures.

Temperature	R_s/Ω	R_{ct}/Ω
−5 °C	0.958	2.822
25 °C	0.833	1.909
60 °C	0.783	1.313

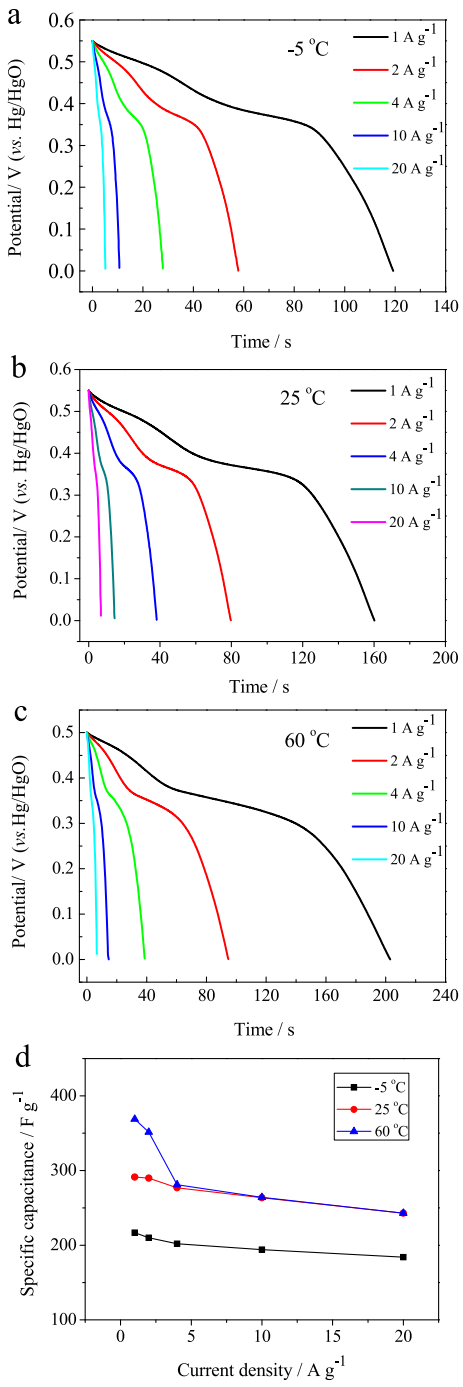

Fig. 7. The first discharge curves of porous Co_3O_4 nanoflake array at: (a) −5 °C, (b) 25 °C, (c) 60 °C; (d) specific capacity of porous Co_3O_4 nanoflake array at different temperatures.

The detailed characteristics of a capacitive electrode can be analyzed by EIS using a Nyquist plot, which represents the imaginary part (Z'') and real part (Z') of impedance [38]. The Nyquist plots of the Co_3O_4 array electrode at different temperatures are presented in Fig. 6b. The impedance spectra are almost similar in

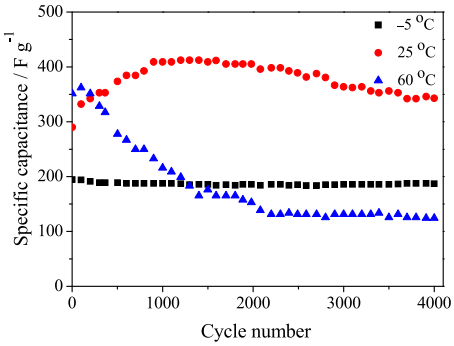

Fig. 8. Cycling performances of porous Co_3O_4 nanoflake arrays at a current density of 2 A g^{-1} at different temperatures.

shape, which consist of a depressed arc in high frequency regions and a straight arc in low frequency regions. Such a plot can be fitted by an equivalent circuit for impedance analysis, and is shown in the inset of Fig. 6b, where R_s represents solution resistance of the electrochemical system, C_{dl} and C_F is a double layer capacitor and a Faradaic pseudocapacitor, respectively; W is Warburg impedance, and R_{ct} represents Faradaic interfacial charge transfer resistance. The solution resistance R_s and the charge transfer resistance R_{ct} can be obtained from the Nyquist plot, where the high frequency semicircle intercepts the real axis at R_s and $(R_s + R_{ct})$, respectively. These parameters are calculated by ZView software and listed in Table 1. It is noticed that both R_s and R_{ct} decrease with the operation temperature. The result has the same tendency with the ionic conductivity of KOH electrolyte that is 85.9, 33.9 and 19.63 ms cm^{-1} at −5 °C, 25 °C and 60 °C, respectively. Increasing the conductivity of electrolyte facilitates the migration of ions towards the electrode materials. And decreasing the charge transfer resistance R_{ct} accelerates the movement of charge inner the Co_3O_4 array electrode.

Fig. 7a–c shows the first charge–discharge profiles of the porous Co_3O_4 nanoflake array electrode at a galvanostatic current density of 2 A g^{-1} at −5 °C, 25 °C and 60 °C, respectively. The shape of the charge/discharge curves presents typical pseudocapacitive behavior and is in agreement with the CV results. The porous nanoflake array exhibits a specific capacitance of 217, 210, 202, 194 and 184 F g^{-1} at 1, 2, 4, 10 and 20 A g^{-1} at −5 °C; 291, 289, 277, 263 and 243 F g^{-1} at 1, 2, 4, 10, and 20 A g^{-1} at 25 °C; 369, 351, 281, 264 and 242 F g^{-1} at 1, 2, 4, 10 and 20 A g^{-1} at 60 °C, respectively. As expected, it shows an increase in capacitance at elevated temperature. It is also noticed that with increasing the discharge current density, the specific capacitance of the capacitor decreases exponentially at elevated temperature. As the current density increases above 2 A g^{-1}, there is no much difference of the specific capacitances porous Co_3O_4 nanoflake array at 25 °C and 60 °C. This phenomenon may be attributed to the amount of Co_3O_4 that take part in the redox reaction. Increasing current density, ions do not have enough time to migrate to the active materials, and then in turn decreases the capacitance. At −5 °C, there are only those outer layer atoms in the nanoflake participating in the reaction, so the current density has a weak influence on the specific capacitance. While at elevated temperature, the inner atoms also tale part in the redox reaction. But the inner materials have no time to react as the current density increases. The temperature behaviors in this work are agreement with that of solid polymer electrolyte [47].

Fig. 8 shows the cycling characteristics of the porous Co_3O_4 array electrode at a charge–discharge current density of 2 A g^{-1} at three different temperatures. Upon initial cycling, the discharge pseudocapacitance of the Co_3O_4 array electrode at 25 °C and 60 °C increase gradually, i.e. the activation process. For that at 60 °C, the discharge capacity decreases quickly after a momentary increase and it is only 124 F g^{-1} remaining after 4000 cycles. At 25 °C, the specific capacity of the Co_3O_4 array electrode increases slowly and then keeps a gentle decrease; it still exhibits a specific capacity of 342 F g^{-1} after 4000 cycles. While the electrode tested at −5 °C, there is almost no activation process and the specific capacity is 187 F g^{-1} after the cycling test. This phenomenon is in agreement with the SEM morphologies of the Co_3O_4 arrays after 4000 cycles as shown in Fig. 9. The SEM images indicate that with increasing the operation temperature, the change of the morphology is more obvious. Fig. 9a shows the morphology of the Co_3O_4 array after cycling at −5 °C. It has nearly no difference with that before cycling

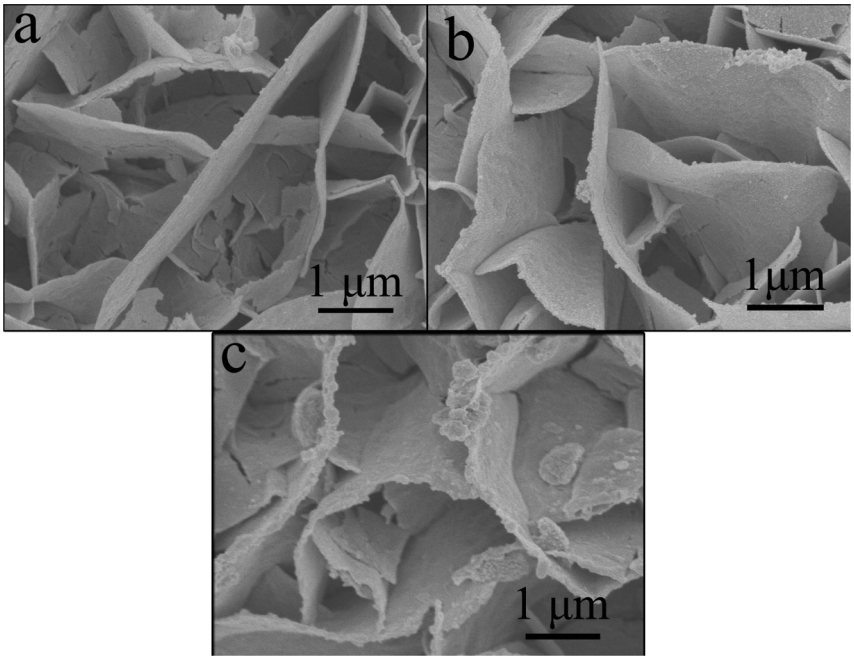

Fig. 9. SEM images of porous Co_3O_4 nanoflake arrays after 4000 cycles operated at different temperatures.

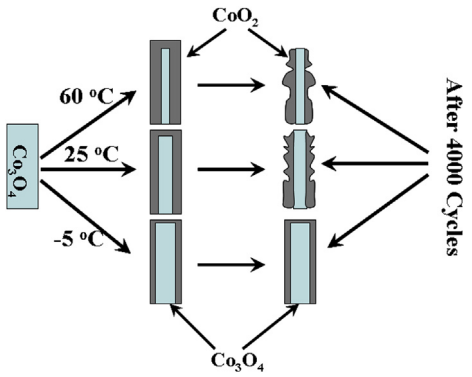

Fig. 10. Schematic degradation mechanism of the porous Co_3O_4 nanoflake array.

as shown in Fig. 2. When tested at 25 °C, the surface is no longer smooth as that of the prime Co_3O_4 nanoflake array and there are many nanoparticles appeared at the edge of the nanoflakes (Fig. 9b). Among the three tested electrodes, changes of the nanoflakes at 60 °C are the most obvious. The nanoflakes are warping and many nanoparticles on the edges are exfoliated (Fig. 9c).

To explain the above electrochemical performance, herein we propose a schematic degradation mechanism of the Co_3O_4 nanoflake array shown in Fig. 10. As the kinetic energy of the migrating ions increases with the operation temperature and the diffusion of ions into micropores of Co_3O_4 electrode may be easier and hence the formation of the reaction layer will be more pronounced. This can result in higher capacitance at elevated temperature. As the current density increases, the Co_3O_4 that takes part in the redox reaction decreases due to the limit of ion diffusion rate. This explains when the current density increases to 4 A g^{-1}, the specific capacity has nearly no difference with that of 25 °C and 60 °C. However, at −5 °C, the pseudo-capacitive reaction only occurs in the surface layer of Co_3O_4 nanoflakes, the operation temperature has little influence on the rate performance. Due to the volume expansion and the oxygen bubble striking during cycling process, the nanoflake array structure has certain extent damage after cycling. The higher the temperature is, the more the Co_3O_4 nanoflakes take part in the pseduo-capacitive reaction, which leading to more serious volume changes. In addition, as shown in Fig. 6a, the oxidation peak moves towards lower potential as the operation temperature increases. Both of the above factors may explain the cycling performance of the porous Co_3O_4 nanoflake array electrode.

4. Conclusions

In summary, a porous Co_3O_4 nanoflake array was fabricated on the Ni foam substrate as an interesting material for pseudocapacitors. The operation temperature has pronounced influence on the electrochemical performance. It shows higher specific capacity while bad cycling performance at 60 °C. On the opposite, at −5 °C, although the specific capacity is not very high, the cycling performance is excellent. It is believed that the above conclusions offer certain guidance for the metal oxide pseduocapacitive reaction in water-based electrolyte.

Acknowledgments

This work is supported by the National Science and Technology Support Program (2012BAC08B08), the Program for Innovative Research Team in University of Ministry of Education of China (IRT13037) and Key Science and Technology Innovation Team of Zhejiang Province (2010R50013).

References

[1] P. Simon, Y. Gogotsi, Nat. Mater. 7 (2008) 845–854.
[2] P. Poizot, S. Laruelle, S. Grugeon, L. Dupont, J.M. Tarascon, Nature 407 (2000) 496–499.
[3] J.R. Miller, P. Simon, Science 321 (2008) 651–652.
[4] J.P. Liu, J. Jiang, C.W. Cheng, H.X. Li, J.X. Zhang, H. Gong, H.J. Fan, Adv. Mater. 23 (2011) 2076–2081.
[5] X.H. Xia, J.P. Tu, X.L. Wang, C.D. Gu, X.B. Zhao, J. Mater. Chem. 21 (2011) 671–679.
[6] C. Liu, F. Li, L.P. Ma, H.M. Cheng, Adv. Mater. 22 (2010) E28–E62.
[7] P. Sharma, T.S. Bhatti, Energy Convers. Manage. 51 (2010) 2901–2912.
[8] R. Vellacheri, V.K. Pillai, S. Kurungot, Nanoscale 4 (2012) 890–896.
[9] C.C. Hu, K.H. Chang, M.C. Lin, Y.T. Wu, Nano Lett. 6 (2006) 2690–2695.
[10] P.R. Deshmukh, S.N. Pusawale, A.D. Jagadale, C.D. Lokhande, J. Mater. Sci. 47 (2012) 1546–1553.
[11] X. Liu, P.G. Pickup, Energy Environ. Sci. 1 (2008) 494–500.
[12] J.M. Ko, K.M. Kim, Mater. Chem. Phys. 114 (2009) 837–841.
[13] A. Yu, A. Sy, A. Davies, Synth. Met. 161 (2011) 2049–2054.
[14] Q. Lu, Y.K. Zhou, J. Power Sources 196 (2011) 4088–4094.
[15] M. Kim, Y. Hwang, J. Kim, J. Power Sources 239 (2013) 225–233.
[16] W. Tang, Y.Y. Hou, X.J. Wang, Y. Bai, Y.S. Zhu, H. Sun, Y.B. Yue, Y.P. Wu, K. Zhu, R. Holze, J. Power Sources 197 (2012) 330–333.
[17 J. Ge, H.B. Yao, W. Hu, X.-F. Yu, Y.-X. Yan, L.B. Mao, H.-H. Li, S.-S. Li, S.-H. Yu, Nano Energy 2 (2013) 505–513.
[18] B.R. Duan, Q. Cao, Electrochim. Acta 64 (2012) 154–161.
[19] X.H. Xia, J.P. Tu, X.L. Wang, C.D. Gu, X.B. Zhao, Chem. Commun. 47 (2011) 5786–5788.
[20] Y.Y. Gao, S.L. Chen, D.X. Cao, G.L. Wang, J.L. Yin, J. Power Sources 195 (2010) 1757–1760.
[21] X.H. Xia, J.P. Tu, Y.Q. Zhang, Y.J. Mai, X.L. Wang, C.D. Gu, X.B. Zhao, RSC Adv. 2 (2012) 1835–1841.
[22] Q. Yang, Z.Y. Lu, Z. Chang, W. Zhu, J.Q. Sun, J.F. Liu, X.M. Sun, X. Duan, RSC Adv. 2 (2012) 1663–1668.
[23] F. Zhang, C.Z. Yuan, X.J. Lu, L.J. Zhang, Q. Che, X.G. Zhang, J. Power Sources 203 (2012) 250–256.
[24] H.-W. Shim, A.H. Lim, J.C. Kim, E. Jang, S.D. Seo, G.H. Lee, T.D. Kim, D.W. Kim, Sci. Rep. 3 (2013). Art. 2325.
[25] W. Du, R.M. Liu, Y.W. Jiang, Q.Y. Lu, Y.Z. Fan, F. Gao, J. Power Sources 227 (2013) 101–105.
[26] J. Zhi, S. Deng, Y.X. Zhang, Y.F. Wang, A.G. Hu, J. Mater. Chem. A 1 (2013) 3171–3176.
[27] S.I. Kim, J.S. Lee, H.J. Ahn, H.K. Song, J.H. Jang, ACS Appl. Mater. Interfaces 5 (2013) 1596–1603.
[28] X.H. Xia, J.P. Tu, Y.J. Mai, R. Chen, X.L. Wang, C.D. Gu, X.B. Zhao, Chem. Eur. J. 17 (2011) 10898–10905.
[29] Y.Q. Zhang, X.H. Xia, J.P. Tu, Y.J. Mai, S.J. Shi, X.L. Wang, C.D. Gu, J. Power Sources 199 (2012) 413–417.
[30] Z.H. Yang, F.F. Xu, W.X. Zhang, Z.S. Mei, B. Pei, X. Zhu, J. Power Sources 246 (2014) 24–31.
[31] M.P. Yeager, D. Su, N.S. Marinkovic, X.W. Teng, J. Electrochem. Soc. 159 (2012) A1598–A1603.
[32] X.H. Xia, J.P. Tu, Y.J. Mai, X.L. Wang, C.D. Gu, X.B. Zhao, J. Mater. Chem. 21 (2011) 9319–9325.
[33] T. Xue, X. Wang, J.-M. Lee, J. Power Sources 201 (2012) 382–386.
[34] J.B. Wu, R.Q. Guo, X.H. Huang, Y. Lin, J. Power Sources 243 (2013) 317–322.
[35] H.N. Zhang, Y.J. Chen, W.W. Wang, G.H. Zhang, M. Zhuo, H.M. Zhang, T. Yang, Q.H. Li, T.H. Wang, J. Mater. Chem. A 1 (2013) 8593–8600.
[36] M.S. Wu, M.J. Wang, Electrochem. Solid State Lett. 13 (2010) A1–A3.
[37] X.H. Xia, J.P. Tu, Y.Q. Zhang, Y.J. Mai, X.L. Wang, C.D. Gu, X.B. Zhao, J. Phys. Chem. C. 115 (2011) 22662–22668.
[38] J.W. Lee, T. Ahn, J.H. Kim, J.M. Ko, J.-D. Kim, Electrochim. Acta 56 (2011) 4849–4857.
[39] S.J. He, C.X. Hu, H.Q. Hou, W. Chen, J. Power Sources 246 (2014) 754–761.
[40] C.-W. Kung, H.-W. Chen, C.-Y. Lin, R. Vittal, K.-C. Ho, J. Power Sources 214 (2012) 91–99.
[41] X.H. Xia, J.P. Tu, Y.Q. Zhang, J. Chen, X.L. Wang, C.D. Gu, C. Guan, J.S. Luo, H.J. Fan, Chem. Mater. 24 (2012) 3793–3799.
[42] M. Shahid, J.L. Liu, I. Shakir, M.F. Warsi, M. Nadeem, Y.U. Kwon, Electrochim. Acta 85 (2012) 243–247.
[43] D. Sarkar, G.G. Khan, A.K. Singh, K. Mandal, J. Phys. Chem. C. 117 (2013) 15523–15531.
[44] T. Zhu, J.S. Chen, X.W. Lou, J. Mater. Chem. 20 (2010) 7015–7020.
[45] S.K. Meher, G.R. Rao, J. Phys. Chem. C. 115 (2011) 15646–15654.
[46] Y. Chen, X. Zhang, D.C. Zhang, P. Yu, Y.W. Ma, Carbon 49 (2011) 573–580.
[47] R.S. Hastak, P. Sivaraman, D.D. Potphode, K. Shashidhara, A.B. Samui, Electrochim. Acta 59 (2012) 296–303.
[48] Y.R. Liang, F.X. Liang, H. Zhong, Z.H. Li, R.E. Fu, D.C. Wu, J. Mater. Chem. A 1 (2013) 7000–7005.
[49] Y.Q. Zhang, X.H. Xia, J. Kang, J.P. Tu, Chin. Sci. Bull. 57 (2012) 4215–4219.
[50] X.H. Xia, J.P. Tu, J.Y. Xiang, X.H. Huang, X.L. Wang, X.B. Zhao, J. Power Sources 195 (2010) 2014–2022.